Journal of Materials Chemistry A

ARTICLE

Decoration of the inert basal plane of defect-rich MoS₂ with Pd atoms for achieving Pt-similar HER activity

Kun Qi, Shansheng Yu, Qiyu Wang, Wei Zhang, Jinchang Fan, Weitao Zheng* and Xiaoqiang Cui*

Outstanding hydrogen evolution reaction (HER) activity and stability are highly desired for transition metal dichalcogenide (TMD)-based catalysts as Pt substitutes. Here, we theoretically calculated and experimentally implemented to show that adsorbing Pd atoms on the basal plane of defect-rich (DR) MoS₂ will effectively modulate the surface electronic state of MoS₂ while retaining its active sites, which greatly enhanced the HER activity. Three decoration strategies were used to implement this design: direct epitaxial growth, assembling spherical nanoparticles and assembling Pd nanodisks (NDs). The results showed that only Pd NDs are able to be site-specifically decorated on the basal plane of DR-MoS₂ through lamellar-counterpart-induced van der Waals pre-combination and covalent bonding. This Pd NDs/DR-MoS₂ heterostructure exhibits exceptional Pt-similar HER properties with a low onset-overpotential (40 mV), small Tafel slope (41 mV dec⁻¹), extremely high exchange current density (426.58 µA cm⁻²) and robust HER durability. These results demonstrate a novel modification strategy by a lamellar metallic nanostructure for designing excellent layered TMD-based HER catalysts.

1. Introduction

The electrocatalytic hydrogen evolution reaction (HER) is an efficient and easily accessible strategy for producing hydrogen,[1, 2] which is considered a promising eco-friendly and sustainable substitute fuel with high energy density.[3, 4] Most of the research on HER in the past few years has been focused on efforts to develop earth-abundant materials to replace the state-of-the-art Pt.[5] Among these alternatives, molybdenum disulfide (MoS₂) has gained tremendous attention because of its high natural abundance and high HER efficiency resulting from its characteristic structure and appropriate hydrogen adsorption energy.[6, 7] Although numerous attempts have been made to improve the HER activity of MoS₂, engineering MoS₂-based electrocatalysts with activities similar to Pt remains challenging.[8-11] Creating additional HER-active sites by designing defect-rich or edge-oriented structures has resulted in superior HER performance because unsaturated terrace and edge sites have been demonstrated to be active sites for the HER reaction.[12-16] Improving the intrinsic conductivity of MoS₂ is another effective approach for enhancing its activity.[9, 17-20] Unfortunately, increasing the number of active sites and enhancing the conductivity are normally contradictory because an abundance of active sites will generally decrease the intrinsic conductivity of MoS₂.[21]

To overcome this obstacle, Xie's group developed oxygen-incorporated disordered MoS₂ ultrathin nanosheets for efficient HER with both abundant active sites and good intrinsic conductivity.[9] Bao's group doped a single Pt atom into a matrix of MoS₂ to improve the electronic state and the inert S-atom activity.[22] Recently, Santos and Nørskov's theoretical studies have predicted that the HER activity of monolayer MoS₂ can be enhanced by adsorbing it onto metal substrates.[23, 24] However, the experimental complexity and the flaws of geometric dimensioning limit the real application of these systems.[25] Modification of metal nanoparticles on MoS₂ nanosheets has already shown a certain enhancement of HER activity.[22, 26-29] Zhang's group has shown that modifying MoS₂ with noble-metal nanoparticles (NPs) can enhance the intrinsic properties of MoS₂.[26] However, these epitaxial growth methods suffer from the fact that the active defect sites are most likely to be covered by the nucleation of the metal nanostructures.[30] Given the aforementioned considerations, successfully modifying the defect-rich MoS₂ nanosheets while retaining their active sites would result in substantial improvement of their HER activity.[21]

Adsorbing Pd atoms on the basal plane of defect-rich MoS₂ will greatly enhance the HER activity because an effectively modulating the surface electronic state of MoS₂ while retaining its active sites based on our theoretical calculations. This MoS₂-based hetero-nanostructure with trace amount of Pd showing Pt-similar HER activity will push forward the real application since the price of Pd is only one third of Pt. Traditional direct epitaxial growth or assembling spherical nanoparticles are not able to meet the requirements of site-

Department of Materials Science, Key Laboratory of Automobile Materials of MOE and State Key Laboratory of Superhard Materials, Jilin University, Changchun 130012 People's Republic of China.
E-mail: xqcui@jlu.edu.cn, wtzheng@jlu.edu.cn

specifically decoration of Pd atoms on the basal plane while retaining the active defect sites of MoS$_2$. Here, we designed and implemented a facile strategy by assembling Pd nanodisks (NDs) on the basal plane of defect-rich MoS$_2$ nanosheets (DR-MoS$_2$) while retaining their active sites. The Pd-ND-modified DR-MoS$_2$ heterostructure (Pd NDs/DR-MoS$_2$) was constructed by the lamellar-counterpart-induced van der Waals pre-combination and further sonication-induced covalent bonding.[31-33] The ingenious assembly strategy and disk-like 2D structure of Pd NDs avoid the occupation of HER active sites which was commonly resulted by traditional epitaxial growth and assembling method. Meanwhile, the surface state of the MoS$_2$ was rationally modulated by Pd-ND modification, resulting in a product that exhibits extremely high HER activity and stability similar to that of Pt/C. Our results demonstrate a potential strategy via lamellar metallic nanostructure modification for designing excellent layered transition metal dichalcogenide (TMD) HER catalysts.

2. Result and discussion

Density functional theory (DFT) calculations were used to predict the surface-state modulation of MoS$_2$ after Pd adsorption. Geometrical optimizations of the palladium-adsorbed MoS$_2$ slab are performed for one palladium atom located near the Mo-edge with sulfur monomers. The three sites of high symmetry are considered, which are top of Mo, S, and hexagon center. It is found when the palladium atom is on the top of S, it will spontaneously fall into its next top of Mo. Therefore, including the edge of MoS$_2$ slab, there exist seven stable geometrical structures as shown in Figure 1. The palladium adsorption energy ΔE(Pd) can be calculated for evaluating the structural stability using the following equation:

$$\Delta E(\text{Pd}) = E(\text{slab} + \text{Pd}) - E(\text{slab}) - E(\text{Pd}) \quad (1)$$

where E(slab + Pd) is the total energy for the MoS$_2$ slab adsorbed with one palladium atom. E(slab) is the total energy for the pristine MoS$_2$ slab, and E(Pd) is the energy for one palladium atom. The calculated palladium adsorption energies are listed in Table 1. Energy values show that the palladium atom clearly prefers to bond with sulfur monomers on the edge due to uncoordinated sulfur atoms in Figure 1f and Figure 1g, which suggests that the catalytic active sits should be blocked. Therefore, we should endeavor to avoid covering the active site during the preparation of catalysts. Except for the edge, the top of Mo is the following favorable adsorbed site on the surface of MoS$_2$ slab in Figure 1a, where the active sits are kept, which is considered to be favorable and detailed discussed in this work.

As described in Figures 1, Table 1, and Figure S1, the fact that Pd atom prefers to bond with uncoordinated S monomers on the edge will result in a decrease in the number of catalytically active sites.[21, 34] On the contrary, the active sites are supposed to be retained if Pd atoms are adsorbed onto the basal plane of MoS$_2$ (Figure 1a-1e), which is favorable for further improvement of the HER activity. The Gibbs free energy of hydrogen adsorption on the edge S atoms of the basal plane modified Pd-MoS$_2$ slab are then calculated that
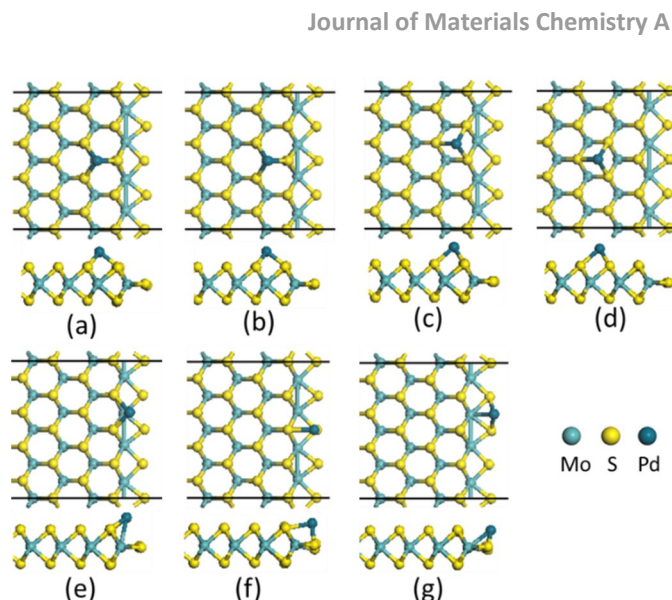

Figure 1. The geometric fragments of palladium adsorbed MoS$_2$ slab. The top and side views of the unit cell of the MoS$_2$ slab are exhibited, in which the Mo-edge is terminated by sulfur monomers.

Table 1. Calculated adsorption energy ΔE_{Pd} for one palladium atom adsorbed on the MoS$_2$ slab.

Figure 1	a	b	c	d	e	f	g
ΔE_{Pd} (eV)	-2.17	-2.10	-2.04	-1.94	-2.11	-2.56	-2.62

possesses a smaller differential binding free energy than that of any pristine MoS$_2$ system previously reported, as shown in Figure 2a, indicating a lower energy barrier or lower overpotential to drive the HER process (see Figures S2, S3 and Tables S1, S2 for details).[6, 9] One notable interesting result is that a much smaller binding free energy obtained at higher H coverage, which indicates that higher H coverage can be achieved at a lower overpotential, thus providing more HER-effective sites on Pd-MoS$_2$ (Figure S4). The density of states (DOS) in Figure 2b show that the electron states near the Fermi level are significantly increased as a result of the adsorption of Pd atoms onto the basal plane of MoS$_2$, which indicates that the electrical conductivity of MoS$_2$ will be enhanced. Benefitting from the optimization of both the H adsorption free energy and the interdomain conductivity of MoS$_2$ by Pd modulation on the basal plane, a better HER performance with a small onset overpotential and large
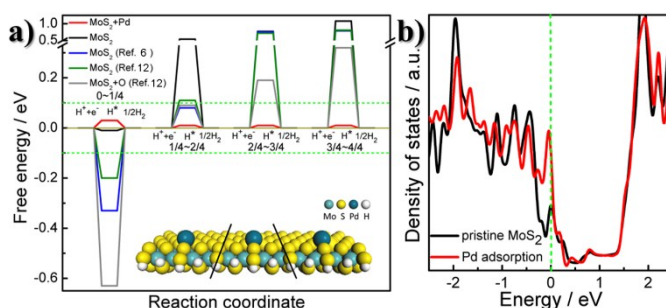

Figure 2. (a) Calculated free-energy diagram for hydrogen evolution at a potential U = 0 relative to the standard hydrogen electrode at pH = 0. The comparison of different MoS$_2$-based materials is taken from ref 6 (blue) and ref 12 (green and gray); (b) Calculated density of states (DOS) of the pristine MoS$_2$ (black) and Pd-adsorbed MoS$_2$ (red).
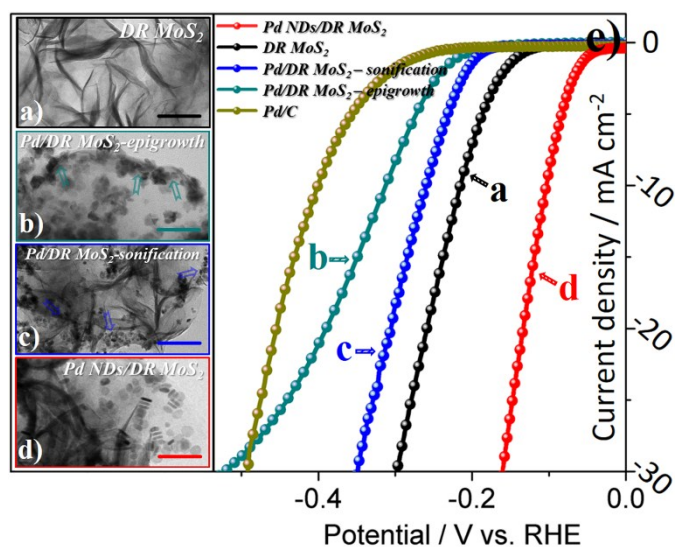
Figure 3. Typical TEM image of (a) DR-MoS$_2$; (b) Pd nanoparticles/DR-MoS$_2$ composite obtained by epitaxial growth method; (c) Pd nanoparticles/DR-MoS$_2$ composite obtained by sonication; (d) Pd NDs/DR-MoS$_2$ (Scale bars: 50 nm; arrows show the aggregation of Pd nanoparticles at the boundary defect sites of DR-MoS$_2$). (e) HER polarization curves of the Pd/DR-MoS$_2$ based catalysts.

Figure 4. (a) Typical TEM image of Pd NDs; the inset in (a) shows the statistical data for diameter and thickness; (b-c) HRTEM images of two Pd NDs recorded parallel and vertical on a TEM grid, respectively; (d) Corresponding SAED pattern of Pd NDs; (e-f) AFM images of Pd NDs; the inset in (f) illustrates the average length and height drawn from the white square zone in (e).

cathodic current density can be expected for the Pd-MoS$_2$ hetero-coordinated catalyst.[35]

Three decoration strategies were used to implement the design of Pd atom modification: direct epitaxial growth, assembling spherical nanoparticles, and assembling Pd NDs. Ultrathin and defect-rich MoS$_2$ nanosheets were synthesized via a previous method reported by Xie's group as shown in Figure 3a and Figure S5.[13] TEM images in Figure 3 show that Pd are efficiently modified onto the pristin DR-MoS$_2$ surface in all three conditions. Electrochemical results in Figure 3e show that the HER activities of Pd/MoS$_2$ heterostructure from direct epitaxial growth (curve *b*) and assembling spherical nanoparticles (curve *c*) are even worse than that of the pristine DR-MoS$_2$ (curve *a*). The reason of the poor performances is explained by the fact that the direct epitaxial growth or assembly of small Pd nanoparticles will occur on the uncoordinated S atoms of the boundary defect sites, as indicated by the arrows in the TEM images of Figure 3b and 3c, which will definitely block the HER-active sites. To address this challenge, we synthesized lamellar Pd NDs for assembling on the basal plane of MoS$_2$ by exploiting the strong van der Waals interaction between two lamellar counterparts.[36] The HER performance of DR-MoS$_2$ is greatly improved after the modification of Pd NDs, as shown by curve *d* in Figure 3e. The Pd loading amount for these three methods are kept same for comparison.

Lamellar circular Pd NDs were specially synthesized through a modified solvothermal method in which oxygen was used as an etchant.[37] The structure was characterized by transmission electron microscopy (TEM), high-resolution transmission electron microscopy (HRTEM), selected-area electron diffraction (SAED), and atomic force microscopy (AFM) a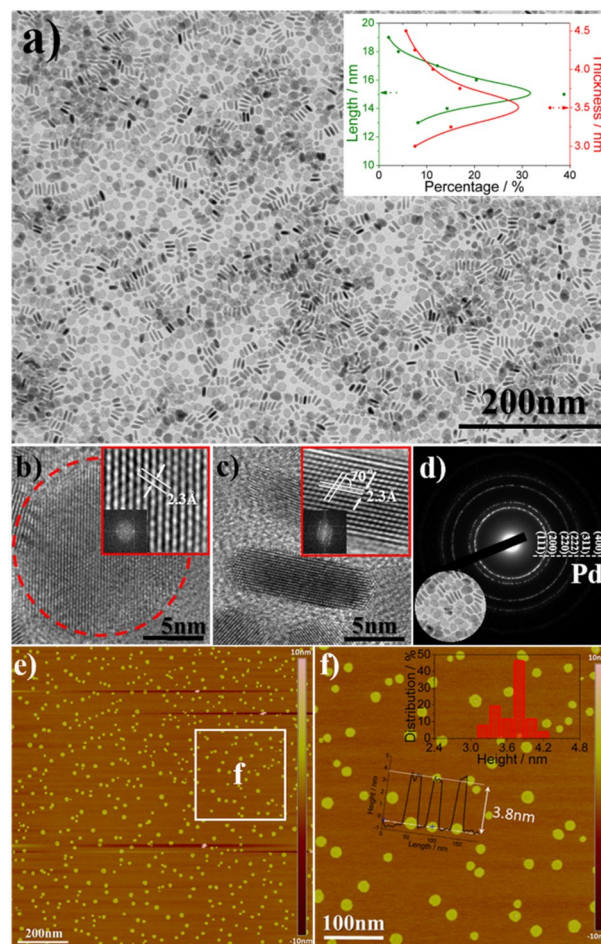s shown in Figure 4. Two main morphologies of nanodisk and nanorod were observed in Figure 4a. The TEM images collected at various tilt angles (Figure S6) suggested that the nanorods are probably the vertical alignment of nanodisks. The disk feature of as-prepared Pd nanostructure is further confirmed by the AFM images in Figure 4e and 4f. HRTEM micrographs and SAED patterns in Figure 4b-4d show that the Pd NDs are dominated by {111} facets. The synergetic effect of etching-regrowth by oxygen and carbon monoxide is demonstrated to be essential during the synthesis of Pd NDs (details are described in SI, Figure S7-S9).[38, 39] The Pd NDs show an average thickness of 3.5 ± 0.9 nm and a diameter of 15.0 ± 3.5 nm.

The Pd NDs/MoS$_2$ hetero-nanostructure were further investigated by TEM, HRTEM, scanning electron microscopy (SEM), energy dispersive X-ray spectrum (EDX), and X-ray photoelectron spectroscopy (XPS). TEM characterization show that the Pd NDs were uniformly assembled on the basal plane of DR-MoS$_2$ (Figure 5a), with seldom aggregating on the boundary defect sites. The combination of Pd NDs and DR-MoS$_2$ was further confirmed by the XRD and HRTEM images in
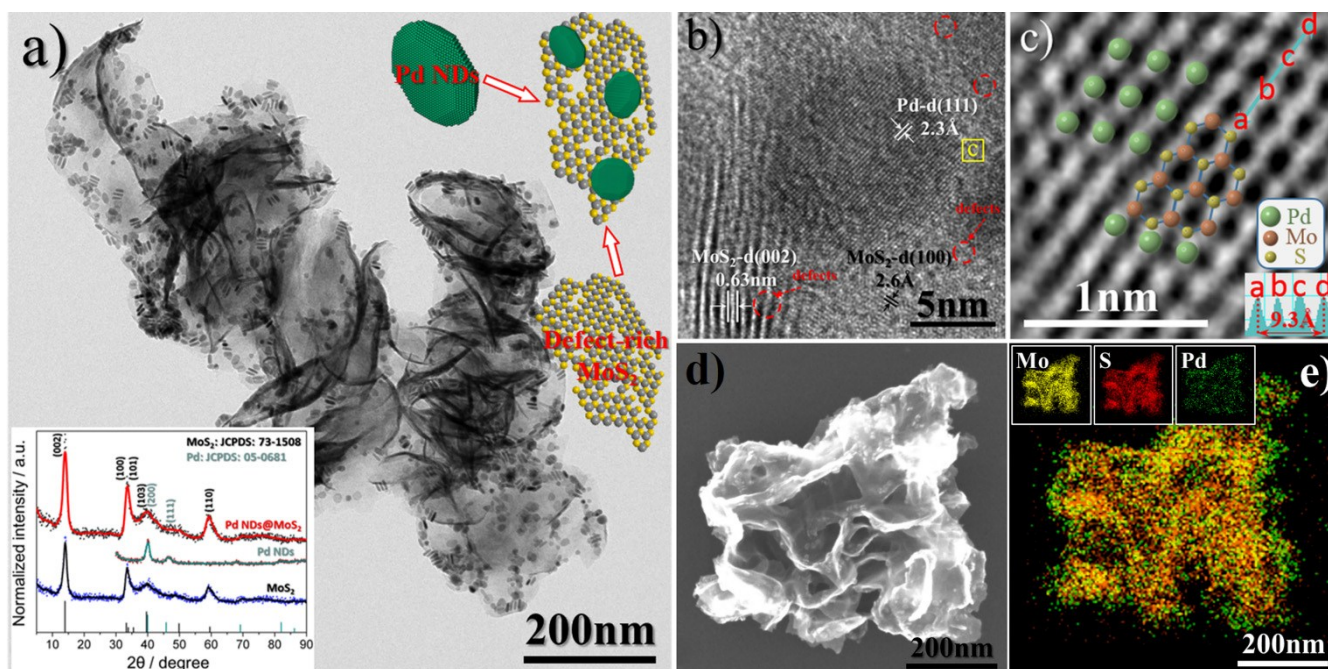
ARTICLE

Figure 5. Characterization of the Pd NDs/DR-MoS$_2$ heterostructure: (a) Typical TEM image of Pd NDs/DR-MoS$_2$; the inset in (a) shows the XRD pattern and the distribution of Pd NDs/DR-MoS$_2$; (b) HRTEM image of the Pd NDs/DR-MoS$_2$; (c) FFT-masked HRTEM image of the yellow square area in (b), which clearly shows the atom distribution of Mo, S and Pd on the surface of the Pd NDs/DR-MoS$_2$; (d) SEM image of Pd NDs/DR-MoS$_2$; (e) EDX mapping image of Pd NDs/DR-MoS$_2$; inset in (e) show the element distribution of Mo, S and Pd, respectively.

Figure 5a and 5b, respectively. The boundary between the {111} facet arranged Pd atoms and the hexagonally arranged Mo and S atoms is evident in the FFT-masked HRTEM image in Figure 5c, which shows a tight morphological combination between the counterparts.[40, 41] SEM (Figure 5d) and EDX mapping (Figure 5e) data further confirmed the uniform distribution of Pd NDs on DR-MoS$_2$ nanosheets, which may be benefit for adjusting the surface electronic state of MoS$_2$. Weak van der Waals interactions between the two lamellar structures are presumed to benefit the assembly of the Pd NDs on the MoS$_2$ nanosheets.[31, 42] Sonication is essential to overcoming the slight electrostatic repulsions because both the Pd NDs and MoS$_2$ are negatively charged (Figure S10-S11). The coefficient of the van der Waals pre-interaction and subsequent high-speed jets or intense shock waves induced by cavitation may facilitate the formation of covalent bonds between Pd and S for self-assembly.[34, 43]
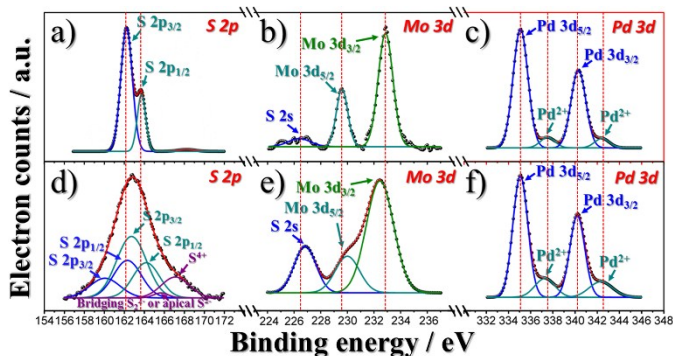

Figure 6. XPS spectra showing the surface binding state of (a-b) DR-MoS$_2$ nanosheets; (c) Pd NDs and (d-f) Pd NDs/DR-MoS$_2$.

The XPS data presented in Figure 6 show that the covalent bonds are formed between Pd and S atoms after the modification. The binding energies of Mo and S in the MoS$_2$ nanosheets exhibit an obvious variation before (Figure 6a and 6b) and after (Figure 6d and 6e) the Pd ND modification. The S 2p spectrum in Figure 6d shows a broad and complex peak consisting of three doublets, i.e., S^{2-} 2p$_{3/2}$ (160.2 eV), S^{2-} 2p$_{1/2}$ (162.3 eV); S$_2^{2-}$ 2p$_{3/2}$ (162.9 eV), S$_2^{2-}$ 2p$_{1/2}$ (164.4 eV); and bridging S$_2^{2-}$ or/and apical S^{2-} (165.5 eV), S^{4+} (166.9 eV).[16, 44] The appearance of S with a high binding energy state may indicate potential HER-active sites.[11, 20, 45] The binding energy of the Mo 3d spectrum also shows an obvious shift of the peak position (Figure 6b and 6e), which is attributed to the valence-state variation of Mo stemming from the bonding between S and Pd after the Pd ND modification.[46-48] A comparison of the Pd 3d spectra (Figure 6c and Figure 6f) reveals a slight Pd^0 positive shift and the appearance of much more Pd^{2+} after combination, which further confirms the formation of covalent bonds between S and Pd during sonication, indicating the tight bonding between the Pd NDs and MoS$_2$ nanosheets.[49] The variations of the S 2p, Mo 3d and Pd 3d spectra after the Pd ND modification clearly show that the surface-state modulation which may further enhance the interdomain conductivity.[50] The variation of the electronic state about S may benefit the HER because the increase in the number of unsaturated sulfide bonds on the intrinsic surface will boost the HER activity.[9, 51] The XPS results obtained from DR-MoS$_2$ sonicated in the absence of Pd NDs shows a negligible change of the surface states (Figure S12).
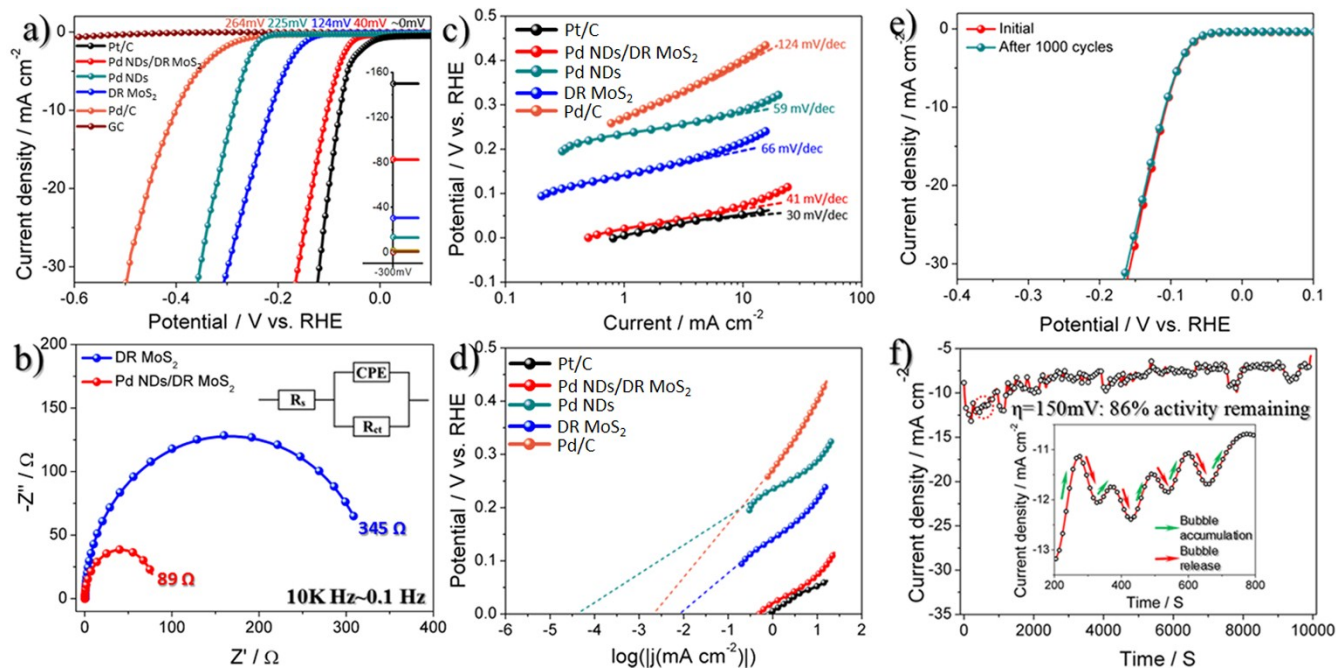
Figure 7. (a) Polarization curves of catalysts tested in N_2-saturated 0.5 M H_2SO_4, along with a bare glassy carbon (GC) electrode, Pt/C, Pd/C, Pd NDs and DR-MoS_2 for comparison; the inset in (a) shows the current density of catalysts at the same overpotential of 300 mV; (b) Nyquist plots for different samples; the fitted curves are represented by solid lines; (c) Tafel plots and (d) exchange current density of various samples calculated using extrapolation methods; (e) Polarization curves revealing that negligible degradation of HER activity is observed for Pd NDs/DR-MoS_2 after 1000 cyclic voltammetry cycles; (f) Time dependence of the current density for Pd NDs/DR-MoS_2 under a static overpotential of 150 mV; the inset in (f) shows the enlargement of the area denoted by the red dashed circle.

The HER activity of Pd NDs/DR-MoS_2 was investigated by electrochemical measurements in 0.5 M H_2SO_4 solution. As-prepared Pd NDs/DR-MoS_2 exhibits an extremely small onset overpotential (η) of 40 mV for the HER, which is much smaller than those of the DR-MoS_2,[9, 51] Pd NDs, and also Pd/C, and is even similar to that of Pt/C. The cathodic current density is 83 mA cm^{-2} at an overpotential of 300 mV, which is 2.8 and 6.4 times greater than those of MoS_2[9, 51] and Pd NDs, respectively (Figure 7a and Table S3). Electrochemical impedance spectroscopy (EIS) characterization of the Nyquist plots (Figure 7b) reveals that the Pd NDs/DR-MoS_2 heterostructure shows a remarkable decrease in charge-transfer resistance (R_{ct}) compared with the MoS_2 nanosheets, which is attributed to the enhancement of the interdomain conductivity upon Pd ND modification, consistent with the DOS results illustrated in Figure 2b.[19, 52, 53]

The Tafel plots of various catalysts were constructed to reveal their HER reaction kinetics. The Tafel slope of the Pd NDs/DR-MoS_2 is 41 mV dec^{-1}, as shown in Figure 7c. To the best of our knowledge, this value, which is similar to the 30 mV dec^{-1} of Pt/C, surpasses most of the previously reported Tafel slopes for MoS_2-based materials and is even comparable to those of Pt-MoS_2 hybrids and Pt-NP-modified TiS_2, which exhibit a low slope of 40 mV dec^{-1},[26, 54, 55] indicating a Heyrovsky or Tafel rate-determining-step mechanism for the HER, instead of the common Volmer reaction.[56, 57] The small Tafel slope will lead to a faster increase of the HER rate with increasing overpotential, which is important in practical applications.[58, 59] Exchange current density values of various samples were obtained by applying an extrapolation method

to the Tafel plots (Figure 7d). The Pd NDs/DR-MoS_2 catalyst displays an extremely large exchange current density of 426.58 $\mu A\ cm^{-2}$, which is 50.7 times greater than that of DR-MoS_2 nanosheets (Table S4). These results represent, for the first time, a non-Pt-metal-modulated MoS_2 catalyst that approaches the performance of the benchmark Pt/C catalyst with superior catalytic activity and favorable reaction kinetics compared with catalysts previously reported in the literature, as shown in Table 2.

The cycling stability and long-term durability of Pd NDs/DR-MoS_2 for HER were further studied in acidic media. The linear sweep voltammetry (LSV) curves measured for Pd NDs/DR-MoS_2 before and after 1000 cyclic voltammetry (CV) cycles between 0.1 and -0.3 V vs. RHE at a scan rate of 50 mV s^{-1} exhibit a negligible loss in current density compared to the initial curve (Figure 7e). Figure 7f shows the long-term durability measured by performing a continuous HER at a static overpotential of 150 mV. Consistent H_2 generation was observed during the HER process (Figure S13) as the reaction proceeded. The as-measured time-dependent curve has a zigzag shape that can be attributed to the alternate processes of bubble accumulation and release on the surface of the electrode.[13] The NDs/DR-MoS_2 modified electrode is hydrophilic with a contact angle of 46° that will not affect the electrochemical behavior on the surface (as shown in Figure S14). After scanning was performed for 10,000 seconds, only a slight degradation of current density was observed; this degradation might be caused by the consumption of H^+ in the electrolyte or by H_2 bubbles remaining on the surface of the electrode thus hindering the reaction. The XPS and TEM results

Table 2. Comparison of HER parameters.

Materials	Onset overpotential [mV]	Tafel slope [mV decade^{-1}]	j [mA cm^{-2}][a)]	η [mV][b)]	Reference
Pd NDs/DR-MoS$_2$	40	41	83	103	This work
Pd NDs	249	59	13	286	This work
DR-MoS$_2$	166	66	21	208	This work
Pd/C	264	124	2	398	This work
Pt/C	~0	30	150	77	This work
Defect-rich MoS$_2$	120	50	~65	~190	13
Defect-free MoS$_2$	180	87	~15	~265	13
Bulk MoS$_2$	250	81	~3	N/A	13
Edge-oriented MoS$_2$	150	50	~20	~280	14
Double-gyroid MoS$_2$	~175	50	~11	~230	15
MoS$_2$/RGO	100	41	N/A	~150	17
Metallic MoS$_2$	195	54	~80	~190	18
1T MoS$_2$	100	40	~40	~205	19
MoS$_2$/N-Doped CNT	75	40	N/A	~110	20
Pt atom doped MoS$_2$	~150	96	N/A	~150	22
Au NRs-MoS$_2$ (dark)	220	86	~7	~330	29
Au NRs-MoS$_2$ (bright)	160	71	~20	~260	29
Au-MoS$_2$	230	57	~3	~346	30
PI/RGO/CNT/MoS$_2$	90	103	~21	~220	52
MoO$_3$-MoS$_2$ Nanowires	200	60	~7	~250	57

[a)] Cathodic current density (j) was recorded at η = 300 mV. [b)] Overpotential (η) was recorded at j = 10 mA cm^{-1}

reveal negligible changes of the morphology and composition after the durability tests (Figure S15 and Figure S16).

3. Conclusions

In summary, a newly designed HER catalyst—Pd modified on the basal plane of a DR-MoS$_2$ nanosheet—was determined by DFT calculations to be highly active toward the HER. The heterostructure was implemented by synthesizing and assembling a disk-like Pd nanostructure onto the basal plane of DR-MoS$_2$ while retaining the active sites. The synergistic regulation of both the structure and electronic states caused the Pd-NDs/DR-MoS$_2$ heterostructure to exhibit exceptional HER properties with a low onset-overpotential, small Tafel slope, extremely high exchange current density and robust HER durability. These results represent, for the first time, a non-Pt-metal-modulated MoS$_2$ catalyst that approaches the performance of the benchmark Pt/C catalyst with superior catalytic activity and favorable reaction kinetics compared with catalysts previously reported in the literature. The study demonstrates the potential for HER catalytic performance improvement of layered TMDs by modification of the lamellar metal nanostructure, which will open a new pathway for improving the HER activity of catalysts through synergistic structural and electronic modulations.

Acknowledgements

Notes and references

1. J. D. Benck, T. R. Hellstern, J. Kibsgaard, P. Chakthranont and T. F. Jaramillo, *ACS Catal*, 2014, **4**, 3957-3971.
2. Y. Zheng, Y. Jiao, M. Jaroniec and S. Z. Qiao, *Angew. Chem. Int. Ed.*, 2015, **54**, 52-65.
3. J. A. Turner, *Science*, 2004, **305**, 972-974.
4. M. S. Dresselhaus and I. L. Thomas, *Nature*, 2001, **414**, 332-337.
5. J. Yang and H. S. Shin, *J. Mater. Chem. A*, 2014, **2**, 5979-5985.
6. B. Hinnemann, P. G. Moses, J. Bonde, K. P. Jørgensen, J. H. Nielsen, S. Horch, I. Chorkendorff and J. K. Nørskov, *J. Am. Chem. Soc.*, 2005, **127**, 5308-5309.
7. J. K. Nørskov, T. Bligaard, J. Rossmeisl and C. H. Christensen, *Nat. Chem.*, 2009, **1**, 37-46.
8. M. Zeng and Y. Li, *J. Mater. Chem. A*, 2015, **3**, 14942-14962.
9. J. Xie, J. Zhang, S. Li, F. Grote, X. Zhang, H. Zhang, R. Wang, Y. Lei, B. Pan and Y. Xie, *J. Am. Chem. Soc.*, 2013, **135**, 17881-17888.
10. B. Lassalle-Kaiser, D. Merki, H. Vrubel, S. Gul, V. K. Yachandra, X. Hu and J. Yano, *J. Am. Chem. Soc.*, 2015, **137**, 314-321.
11. H. Vrubel and X. Hu, *ACS Catal*, 2013, **3**, 2002-2011.

12. T. F. Jaramillo, K. P. Jørgensen, J. Bonde, J. H. Nielsen, S. Horch and I. Chorkendorff, *Science*, 2007, **317**, 100-102.
13. J. Xie, H. Zhang, S. Li, R. Wang, X. Sun, M. Zhou, J. Zhou, X. W. D. Lou and Y. Xie, *Adv. Mater.*, 2013, **25**, 5807-5813.
14. Y. Yang, H. Fei, G. Ruan, C. Xiang and J. M. Tour, *Adv. Mater.*, 2014, **26**, 8163-8168.
15. J. Kibsgaard, Z. Chen, B. N. Reinecke and T. F. Jaramillo, *Nat. Mater.*, 2012, **11**, 963-969.
16. X. Ge, L. Chen, L. Zhang, Y. Wen, A. Hirata and M. Chen, *Adv. Mater.*, 2014, **26**, 3100-3104.
17. Y. Li, H. Wang, L. Xie, Y. Liang, G. Hong and H. Dai, *J. Am. Chem. Soc.*, 2011, **133**, 7296-7299.
18. M. A. Lukowski, A. S. Daniel, F. Meng, A. Forticaux, L. Li and S. Jin, *J. Am. Chem. Soc.*, 2013, **135**, 10274-10277.
19. D. Voiry, M. Salehi, R. Silva, T. Fujita, M. Chen, T. Asefa, V. B. Shenoy, G. Eda and M. Chhowalla, *Nano Lett.*, 2013, **13**, 6222-6227.
20. D. J. Li, U. N. Maiti, J. Lim, D. S. Choi, W. J. Lee, Y. Oh, G. Y. Lee and S. O. Kim, *Nano Lett.*, 2014, **14**, 1228-1233.
21. Y. Sun, S. Gao, F. Lei and Y. Xie, *Chem. Soc. Rev.*, 2015, **44**, 623-636.
22. J. Deng, H. Li, J. Xiao, Y. Tu, D. Deng, H. Yang, H. Tian, J. Li, P. Ren and X. Bao, *Energy Environ. Sci.*, 2015, **8**, 1594-1601.
23. W. Chen, E. J. Santos, W. Zhu, E. Kaxiras and Z. Zhang, *Nano Lett.*, 2013, **13**, 509-514.
24. C. Tsai, F. Abild-Pedersen and J. K. Nørskov, *Nano Lett.*, 2014, **14**, 1381-1387.
25. Y. Tan, P. Liu, L. Chen, W. Cong, Y. Ito, J. Han, X. Guo, Z. Tang, T. Fujita and A. Hirata, *Adv. Mater.*, 2014, **26**, 8023-8028.
26. X. Huang, Z. Zeng, S. Bao, M. Wang, X. Qi, Z. Fan and H. Zhang, *Nat. Commun.*, 2013, **4**, 1444.
27. T. Sreeprasad, P. Nguyen, N. Kim and V. Berry, *Nano Lett.*, 2013, **13**, 4434-4441.
28. L. Yuwen, F. Xu, B. Xue, Z. Luo, Q. Zhang, B. Bao, S. Su, L. Weng, W. Huang and L. Wang, *Nanoscale*, 2014, **6**, 5762-5769.
29. Y. Shi, J. Wang, C. Wang, T. T. Zhai, W. J. Bao, J. J. Xu, X. H. Xia and H. Y. Chen, *J. Am. Chem. Soc.*, 2015, **137**, 7365-7370.
30. J. Kim, S. Byun, A. J. Smith, J. Yu and J. Huang, *J. Phys. Chem. Lett.*, 2013, **4**, 1227-1232.
31. C. H. Lee, G. H. Lee, A. M. van der Zande, W. C. Chen, Y. L. Li, M. Y. Han, X. Cui, G. Arefe, C. Nuckolls, T. F. Heinz, J. Guo, J. Hone and P. Kim, *Nat. Nanotechnol.*, 2014, **9**, 676-681.
32. Y. Shi, W. Zhou, A. Y. Lu, W. Fang, Y. H. Lee, A. L. Hsu, S. M. Kim, K. K. Kim, H. Y. Yang and L. J. Li, *Nano Lett.*, 2012, **12**, 2784-2791.
33. C. Gong, C. Huang, J. Miller, L. Cheng, Y. Hao, D. Cobden, J. Kim, R. S. Ruoff, R. M. Wallace and K. Cho, *ACS Nano*, 2013, **7**, 11350-11357.
34. J. C. Love, D. B. Wolfe, R. Haasch, M. L. Chabinyc, K. E. Paul, G. M. Whitesides and R. G. Nuzzo, *J. Am. Chem. Soc.*, 2003, **125**, 2597-2609.
35. Y. Jiao, Y. Zheng, M. Jaroniec and S. Z. Qiao, *Chem. Soc. Rev.*, 2015, **44**, 2060-2086.
36. A. Tkatchenko, *Adv. Funct. Mater.*, 2014, **25**, 2054-2061.
37. X. Huang, S. Tang, X. Mu, Y. Dai, G. Chen, Z. Zhou, F. Ruan, Z. Yang and N. Zheng, *Nat. Nanotechnol.*, 2011, **6**, 28-32.
38. M. Liu, Y. Zheng, L. Zhang, L. Guo and Y. Xia, *J. Am. Chem. Soc.*, 2013, **135**, 11752-11755.
39. M. N. O'Brien, M. R. Jones, K. L. Kohlstedt, G. C. Schatz and C. A. Mirkin, *Nano Lett.*, 2015, **15**, 1012-1017.
40. K. Wang, J. Wang, J. Fan, M. Lotya, A. O'Neill, D. Fox, Y. Feng, X. Zhang, B. Jiang and Q. Zhao, *ACS Nano*, 2013, **7**, 9260-9267.
41. P. F. Siril, L. Ramos, P. Beaunier, P. Archirel, A. Etcheberry and H. Remita, *Chem. Mater.*, 2009, **21**, 5170-5175.
42. A. K. Geim and I. V. Grigorieva, *Nature*, 2013, **499**, 419-425.
43. H. Xu, B. W. Zeiger and K. S. Suslick, *Chem. Soc. Rev.*, 2013, **42**, 2555-2567.
44. H. Vrubel, D. Merki and X. Hu, *Energy Environ. Sci.*, 2012, **5**, 6136-6144.
45. C. G. Morales-Guio and X. Hu, *Acc. Chem. Res.*, 2014, **47**, 2671-2681.
46. H. T. Wang, C. Tsai, D. S. Kong, K. R. Chan, F. Abild-Pedersen, J. Norskov and Y. Cui, *Nano Res*, 2015, **8**, 566-575.
47. X. Hong, J. Liu, B. Zheng, X. Huang, X. Zhang, C. Tan, J. Chen, Z. Fan and H. Zhang, *Adv. Mater.*, 2014, **26**, 6250-6254.
48. C. G. Morales-Guio, S. D. Tilley, H. Vrubel, M. Gratzel and X. L. Hu, *Nat. Commun.*, 2014, **5**, 3059.
49. A. L. Wang, H. Xu, J. X. Feng, L. X. Ding, Y. X. Tong and G. R. Li, *J. Am. Chem. Soc.*, 2013, **135**, 10703-10709.
50. W. Cui, N. Cheng, Q. Liu, C. Ge, A. M. Asiri and X. Sun, *ACS Catal*, 2014, **4**, 2658-2661.
51. S. S. Chou, Y. K. Huang, J. Kim, B. Kaehr, B. M. Foley, P. Lu, C. Dykstra, P. E. Hopkins, C. J. Brinker and J. Huang, *J. Am. Chem. Soc.*, 2015, **137**, 1742-1745.
52. Y. Jiang, X. Li, S. Yu, L. Jia, X. Zhao and C. Wang, *Adv. Funct. Mater.*, 2015, **26**, 3761-3766.
53. T. Wang, J. Zhuo, K. Du, B. Chen, Z. Zhu, Y. Shao and M. Li, *Adv. Mater.*, 2014, **26**, 3761-3766.
54. Z. Zeng, C. Tan, X. Huang, S. Bao and H. Zhang, *Energy Environ. Sci.*, 2014, **7**, 797-803.
55. J. Kibsgaard, T. F. Jaramillo and F. Besenbacher, *Nat. Chem.*, 2014, **6**, 248-253.
56. X. Zhang, F. Meng, S. Mao, Q. Ding, M. J. Shearer, M. S. Faber, J. Chen, R. J. Hamers and S. Jin, *Energy Environ. Sci.*, 2015, **8**, 862-868.
57. Z. Chen, D. Cummins, B. N. Reinecke, E. Clark, M. K. Sunkara and T. F. Jaramillo, *Nano Lett.*, 2011, **11**, 4168-4175.
58. D. Merki and X. Hu, *Energy Environ. Sci.*, 2011, **4**, 3878-3888.
59. C. G. Morales-Guio, L. A. Stern and X. Hu, *Chem. Soc. Rev.*, 2014, **43**, 6555-6569.

Table of contents

Pd NDs/DR-MoS₂ heterostructure for HER
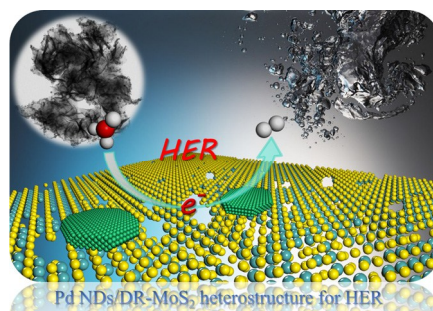
Molybdenum disulfide/palladium nanodisks heterostructure was determined to be highly active toward HER through DFT predictions and experimental verification.